THE ASTROPHYSICAL JOURNAL, 508:736–743, 1998 December 1

HUBBLE SPACE TELESCOPE IMAGING OF THE CIRCUMSTELLAR NEBULOSITY OF T TAURI

KARL R. STAPELFELDT,[1] CHRISTOPHER J. BURROWS,[2,3] JOHN E. KRIST,[2] ALAN M. WATSON,[4] GILDA E. BALLESTER,[5] JOHN T. CLARKE,[5] DAVID CRISP,[1] ROBIN W. EVANS,[1] JOHN S. GALLAGHER III,[6] RICHARD E. GRIFFITHS,[7] JEFF J. HESTER,[8] JOHN G. HOESSEL,[6] JON A. HOLTZMAN,[9] JEREMY R. MOULD,[10] PAUL A. SCOWEN,[8] JOHN T. TRAUGER,[1] AND JAMES A. WESTPHAL[11]

Received 1997 December 18; accepted 1998 July 1

ABSTRACT

Short-exposure Planetary Camera images of T Tauri have been obtained using broadband filters spanning the wavelength range 0.55–0.80 μm. The optically visible star lies very close to an arc of reflection nebulosity. The arc's northern arm extends approximately 5″ from the star, while its southwestern arm appears brighter and extends only 2″. The arc shows an approximate symmetry along an axis toward the west-northwest, the direction of Hind's Nebula and the blueshifted molecular outflow. The morphology of the reflected light is similar to models of scattered light within an illuminated, axisymmetric outflow cavity in a circumbinary envelope, viewed $\approx 45°$ from the outflow axis. However, our model images do not successfully account for the amount of limb brightening that is seen. No optical counterpart to the infrared companion is seen to a limiting magnitude of $V = 19.6$, which suggests $A_V > 7$ mag toward this source. There is no evidence for an optical tertiary, to a limiting $\Delta V = 5.1$ mag fainter than the primary, at the position where such an object has been previously reported.

Subject headings: circumstellar matter — ISM: jets and outflows — stars: imaging — stars: individual (T Tauri)

1. INTRODUCTION

T Tauri (HBC 35) has long been considered a prototype pre–main-sequence star (Joy 1945) but is now known to be a very unique system. The variable, optically visible star is one component of a close binary, with a cool infrared companion 0.″7 to the south (Dyck, Simon, & Zuckerman 1982). The companion, known as T Tauri S, has not yet been detected at optical wavelengths even though it produces the greater part of the bolometric luminosity of the system (Ghez et al. 1991). A third star was reported 0.″27 north of the primary (Nisenson et al. 1985), which was apparently confirmed in the infrared (Maihara & Kataza 1991) but not subsequently seen (Gorham, et al. 1992). In addition, two nebulae are associated with T Tau. Burnham's Nebula (HH 255) is an extended structure of reflection and emission centered on the binary and extending as far as 10″. A separate variable reflection nebula, NGC 1555 (Hind's Nebula), is located 30″ to the west.

Evidence for circumstellar material in the T Tau system is provided by far-infrared and millimeter continuum emission. *IRAS* detected the source as PSC 04190+1924. The spectral energy distribution has been modeled with warm circumstellar dust distributed in both a circumprimary disk (Adams, Lada, & Shu 1987) and a more extended circumstellar envelope (Calvet et al. 1994). Recent millimeter interferometry appears to confirm the presence of a circumstellar disk around the optically visible star T Tauri N (Akeson, Koerner, & Jensen 1998; Hogerheijde et al. 1997) with a diameter of less than 100 AU and mass near $10^{-2}\ M_\odot$. Although no millimeter continuum is detected about the companion, midinfrared excesses clearly indicate the presence of circumstellar material there as well (Herbst, Robberto, & Beckwith 1997).

The kinematics of the region surrounding T Tau have been found to be very complex. High-velocity CO emission from the system has been mapped by Schuster, Harris, & Russell (1997) and Levreault (1988) and shows a preponderance of blueshifted emission west of the binary. Near-infrared molecular hydrogen emission is widely distributed throughout Burnham's Nebula in knots and filaments (Herbst et al. 1996; van Langevelde et al. 1994). Optical spectroscopy has provided the most detailed information, with as many as five distinct kinematic components present in the emission-line spectra (Böhm & Solf 1994). These suggest that both the primary and companion drive separate bipolar outflows. The giant Herbig-Haro flow recently discovered to the north and south of the system is believed to trace the outflow from the infrared companion (Reipurth, Bally, & Devine 1997).

Ground-based coronagraphic images (Nakajima & Golimowski 1995; Robberto et al. 1995) have revealed the structure of Burnham's Nebula outside a radius of 2″ (300 AU). In hopes of detecting the companion star directly in the optical, and of resolving the circumstellar nebulosity to clarify the distribution of material with 2″ of the binary, we have observed T Tau with the *Hubble Space Telescope*

[1] Jet Propulsion Laboratory, MS 183-900, 4800 Oak Grove Drive, Pasadena, CA 91109; krs@wfpc2-mail.jpl.nasa.gov.
[2] Space Telescope Science Institute, 3700 San Martin Drive, Baltimore, MD 21218.
[3] Astrophysics Division, Space Science Department, European Space Agency.
[4] Instituto de Astronomía UNAM, 58090 Morelia, Michoacan, Mexico.
[5] University of Michigan, AOSS-Space Research Lab, 2455 Hayward Street, Ann Arbor, MI 48109.
[6] Department of Astronomy, University of Wisconsin, 475 North Charter Street, Madison, WI 53706.
[7] Carnegie-Mellon University, Department of Physics, 5000 Forbes Avenue, Pittsburgh, PA 15213.
[8] Arizona State University, Department of Physics and Astronomy, Tyler Mall, Tempe, AZ 85287.
[9] Department of Astronomy, New Mexico State University, Box 30001, Department 4500, Las Cruces, NM 88003.
[10] Mt. Stromlo and Siding Springs Observatories, Australian National University, Weston Creek Post Office, ACT 2611 Australia.
[11] Division of Geological and Planetary Sciences, MS 170-25, Caltech, Pasadena, CA 91125.

(*HST*). We report on the observations and results in §§ 2 and 3 and then develop a scattered light model for the reflection nebulosity in § 4.

2. OBSERVATIONS

Three images of T Tau were obtained on 1994 March 4 using the Wide Field and Planetary Camera 2 (WFPC2; Burrows 1995) aboard the *HST*. The star was imaged in the f/28.3 Planetary Camera (PC), in which the 0.″05 FWHM point-spread function (PSF) of *HST* at $\lambda = 555$ nm is sampled at 0.″046 per pixel. The filters and exposure times were F555W, 14 s; F675W, 5 s; and F814W, 3 s. These filters are analogs of the Johnson V, R, and I passbands, respectively. A gain setting of 14 electrons per DN was used to maximize the dynamic range in the data. Image processing steps included subtraction of bias levels derived from rows 8–14 of the overscan, subtraction of a superbias image, subtraction of a composite dark frame scaled to the individual exposure times, the removal of cosmic rays via replacement of affected pixels by a local median, and flat-fielding. We adopt the photometric calibration of Holtzman et al. (1995). Most regions of the image are read-noise limited. In these areas, the short exposure times and small pixel size combine to produce 3 σ limiting surface brightnesses of only 17.8, 16.3, and 15.3 mag arcsec^{-2} in the F555W, F675W, and F814W images, respectively. Close to the star, the limiting surface brightness magnitude is lower because of the difficulty of exactly subtracting the stellar PSF.

3. RESULTS

The F555W reduced image of T Tau is shown in Figure 1, upper left panel. The images are saturated within 0.″1 of the star in all three filters, which has resulted in some bleeding of excess charge up and down the CCD columns (left and right as seen in the figure). The stellar image includes prominent diffraction spikes at 45° angles and the PSF skirt that fades with distance from the stellar position. A faint near-focus point-source image is present 0.″9 northeast of the star superposed on circumstellar nebulosity. The location and brightness of this feature are consistent with an expected ghost image originating when light from T Tau is reflected from the primary image on the CCD and returned to the CCD by an additional reflection from the curved CCD field

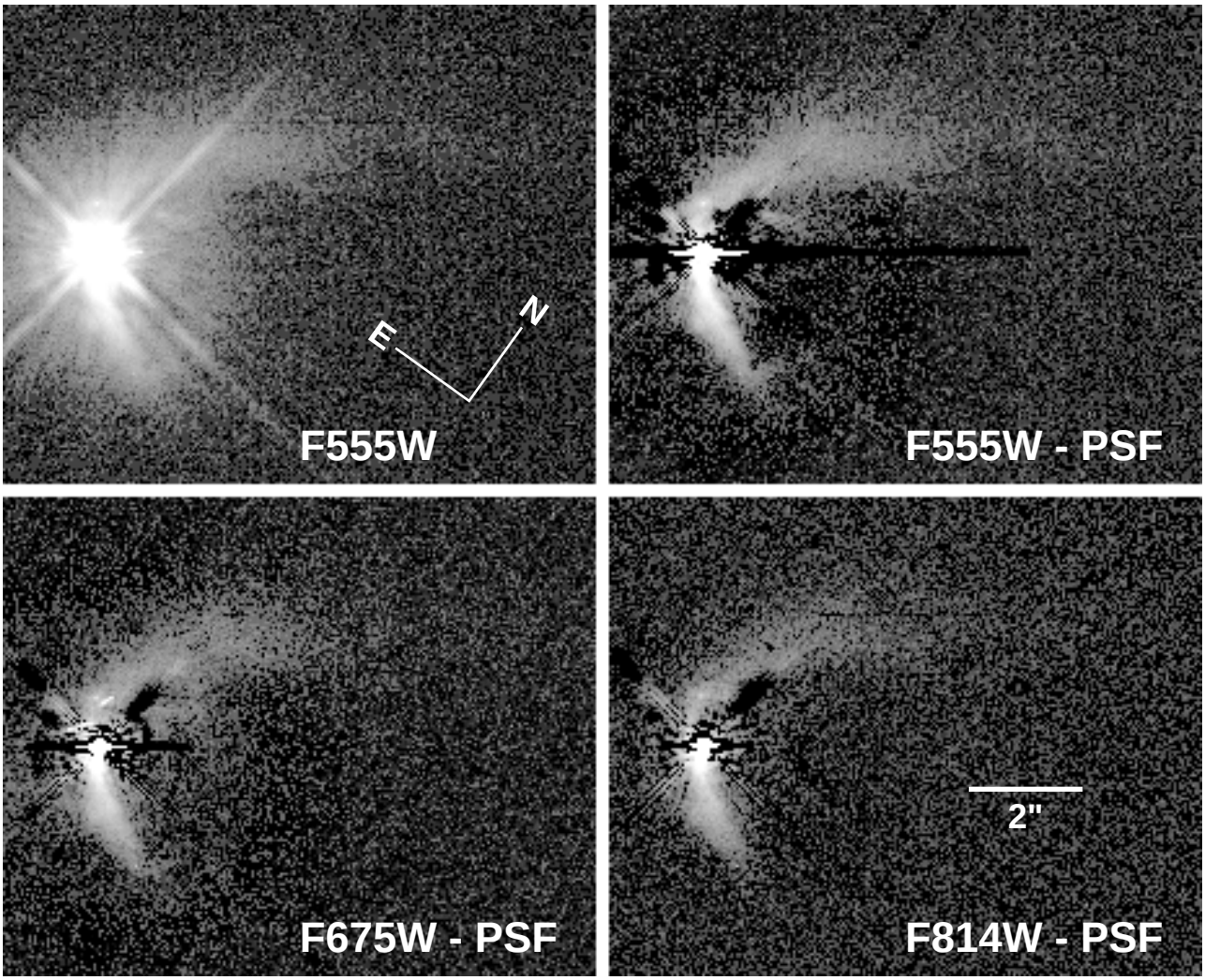

FIG. 1.—Gray-scale WFPC2 images of T Tau showing the star and circumstellar nebulosity. The reduced PC1 F555W image is shown at top left. This same image is shown after subtraction of a scaled and aligned PSF in the top right panel. Similar PSF-subtraction results are obtained for the F675W and F814W images shown in the bottom two panels. In the difference images, saturated pixels in the images of T Tau and the PSF star result in bright and dark horizontal lines running through the stellar position. P.A. 35° points up on the figure; the field of view is 12″ × 10″.

flattener. In the WFPC2 cameras, these ghosts appear offset from the saturated star along a direction oriented away from the field center.

There are two features that are not part of the PSF structure and appear in all three passbands. These are filaments of nebulosity that extend to the upper right and lower right (north and southwest) in Figure 1, upper left panel.

The circumstellar nebular structure can be seen more clearly when a reference PSF is subtracted from the images. Two approaches were tried; the relative merits of each are discussed further by Krist et al. (1997). The first used idealized theoretical PSFs (TinyTIM; Krist 1995) calculated for these filters at the field position of T Tau in the science images. This approach did not produce the best result, because the model does not include known scattering effects at the CCD detector. The second approach was to use saturated WFPC2 stellar images taken in the same filters for reference PSFs. Images of the weak line T Tauri star SAO 76411A, which was found to lack any circumstellar nebulosity, were used. These subtraction results are somewhat better and are shown in Figure 1, upper right and bottom panels, for each of the three filters. In both cases, the alignment and normalization of the reference PSF were accomplished by minimizing the brightness of the symmetric PSF skirt in the difference images. Saturated pixels in both the target and reference PSF images were given zero weight during optimization of the subtraction. Neither the theoretical nor the observed PSFs allow a perfect subtraction free of artifacts; the best difference images still show low-level residual diffraction spikes that confuse the view of the circumstellar features at position angles (P.A.s) 80°, 170°, 260°, and 350°. In addition, saturation column bleeding in the images of T Tau and the observed PSF star obscures the region closest to the star at P.A.s 125° and 305°. Affected pixels lie within the dark horizontal band in Figure 1, upper right and bottom panels.

The subtracted images show that the nebulosity has the form of a continuous, roughly parabolic arc that is concave open to the west-northwest and has a thickness of 0.″5–1.″0. A contour map of the F555W surface brightness is shown in Figure 2. The arc is more closely centered on the primary star than on the infrared companion. T Tau N is positioned near the inside edge of the arc and offset by about 0.″3. The arc is brightest immediately adjacent to the primary and falls rapidly in surface brightness until it is lost in the read noise at the limiting surface brightnesses quoted above. T Tau S lies just outside of the arc, displaced from the arc's center of symmetry and region of maximum brightness. The arc is not symmetrical about the optically visible star. The nebulosity is significantly brighter on the southwest side of the star compared with the northwest side at the same distance. Conversely, the northwest arm of the arc is much longer than that to the southwest, is somewhat wider, and is more curved. The northwest arm extends 5″ from the star in F555W but only about 4″ in the other two filters, because their limiting magnitude is lower. The southwest arm is only 2.″8 long, has more sharply defined edges, and has the same length in all three passbands. This suggests that edges of the southwest arm are defined by the intrinsic source structure and not by the sensitivity level in the images. Note the small "island" of nebulosity present within the nebular arc, approximately 1.″3 north-northwest of T Tau N. This is a real source feature well-separated from the diffraction spike residuals. It is appears in the F555W image but not at

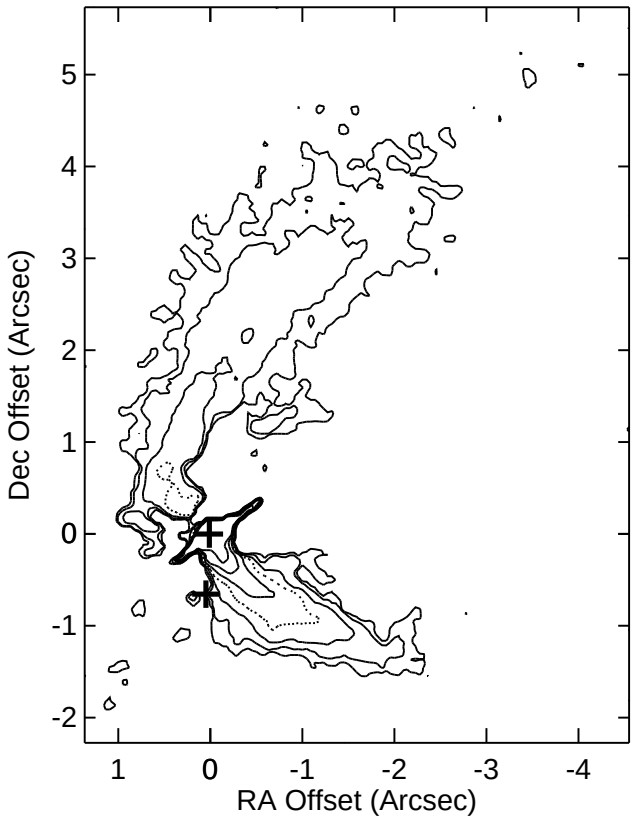

FIG. 2.—Surface brightness map of the WFPC2 F555W image of T Tau. An observed PSF was subtracted from the image. The dotted contour level is 15 mag arcsec^{-2}, and contours are separated by 1 mag arcsec^{-2}. In this figure, north is up, and east is to the left. Locations of the primary star and infrared companion are indicated by the two crosses. Offsets positions are with respect to the primary.

F675W and F814W; this is most likely because of the lower sensitivity of the latter images.

No major color differences are seen within the nebular arc between the three wavelengths that were observed. The brightest Herbig-Haro emission lines in Burnham's Nebula are Hα, [S II], and [O I] (Solf, Böhm, & Raga 1988), all of which fall in the bandpass of the F675W filter. If these lines contributed significantly to the nebular morphology seen by *HST*, they would produce clear morphological differences between the F675W and F814W images. The lack of features unique to the F675W filter strongly argues that the arc is primarily reflection nebulosity in all three bandpasses. A careful comparison of the F555W and F814W images reveals that the inner edge of the northwest arm is bluer than the arm as a whole, while its outer edge may be redder. It is hard to quantify these gradients, because they occur where the signal levels are only a few data numbers. There is no evidence for any color gradient in the southwest arm. Longer exposures are needed to confirm the color gradients in the northwest arm and to detect any of the Herbig-Haro emission knots known to be associated with the system.

The nebula seen in the *HST* images appears to be the inner portion of a larger arc seen in the ground-based measurements of Nakajima & Golimowski (1995) and Robberto et al. (1995). The latter observations extend to much fainter levels (about 22 mag arcsec^{-2}) but provide no data beneath the 2″ radii occulting masks used and have an order of magnitude less spatial resolution. Both groups show that

the northwest arm continues to gently curve outward in the same direction, to grow in width, and to fade in surface brightness away from the star. They also agree that at low surface brightness levels, the southwest arm appears to abruptly change direction from the southwest course that we observe to the southeast. This behavior is not seen in the *HST* images because the brightness of the southeast extension lies below the sensitivity level of our observations ($V = 17.8$ mag arcsec^{-2}).

Photometric measurements of T Tau N are required to quantify the relative brightness of circumstellar features in comparison with the direct starlight. The star is saturated in all the *HST* images, but useful photometry can still be obtained using the calibration of the WFPC2 CCD well depths given by Gilliland (1994). The total number of detected photoelectrons is a sum of the counts outside the saturation region and the number of saturated pixels multiplied by the well depth. A 128 pixel (5.″8) square aperture was used to include all of the brightest nebulosity. We obtain integrated magnitudes (star + nebula) of 10.06, 9.40, and 8.82 in the F555W, F675W, and F814W bandpasses. We estimate the systematic errors at ± 0.05 mag. We find that the total integrated brightness of the reflection nebulosity is about 20% of the direct starlight from T Tau N in all three colors. The F555W magnitude of the system is in reasonable agreement with published ground-based V magnitudes; however, the F555W$-$F675W and F555W$-$F814W colors are about 0.1 and 0.3 mag bluer than the corresponding ground-based $V-R$ and $V-I$ colors (Kenyon & Hartmann 1995; Strom et al. 1989). Color corrections to the WFPC2 photometric system are not large enough to resolve this discrepancy (Holtzman et al. 1995), and thus an intrinsic variation in source color is indicated.

To establish limiting magnitudes for companion stars, PC PSFs of various amplitudes were added into the images at the positions of T Tau S and the supposed optical tertiary. For each image a scaling level for the PSF was determined below which the PSF became indistinguishable by eye against the local background noise. For the infrared companion, this leads to the following WFPC2 limiting magnitudes: $V > 19.6$, $R > 18.2$, and $I > 17.4$. For the supposed optical tertiary, our limiting magnitude is only $V > 15.3$ because of the greater noise from the PSF wings very close to T Tau N.

4. DISCUSSION

4.1. *Constraints on Companion Stars*

No optical counterpart to T Tau S is seen in these images to a limiting magnitude $V > 19.6$, and thus this object is at least 9.5 mag fainter than T Tau N at this wavelength. Unfortunately, this observation only weakly constrains the visual extinction toward the infrared companion. A simple blackbody stellar photosphere corresponding to the post-outburst K magnitude and minimum luminosity of T Tau S (6.5 mag and 15 $L_\odot$; Ghez et al. 1991) would have a $V = 9.6$. The actual spectral energy distribution is certainly more complex, with veiling emission and thermal dust continuum contributing significant excesses above the stellar photosphere. Thus it is difficult to say with certainty what intrinsic V magnitude should be expected for this source. A limiting case that allows the faintest possible intrinsic V magnitude would be a very cool stellar photosphere (log $T_{\rm eff} = 3.5$) combined with a large veiling factor of 4 at $\lambda = 2.2$ μm. Using the observed K magnitude, these assumptions would imply a photospheric $V = 12.5$ and luminosity of 2 $L_\odot$. Thus we suggest the visual extinction toward T Tau S is at least 7 mag. This limit lies at the upper edge of the extinction range ($4 < A_V < 7$) estimated by Ghez et al. (1991) from the strength of the silicate absorption.

There is no evidence in our images for the optical tertiary star reported by Nisenson et al. (1985) and Maihara & Kataza (1991). At the position reported for this source our images are dominated by PSF artifacts from the bright primary, and thus our limiting magnitude is only $\Delta V = 5.2$. Nevertheless, this object would have been detected if it had maintained the same brightness and position that had been first reported. Our observations reaffirm the conclusions of Gorham et al. (1992) that this object must have faded by nearly a magnitude since 1984 if the earlier detections are to be considered valid.

4.2. *Nebula Morphology and the Geometry of the T Tau System*

The major nebular feature near the T Tau binary is the arc of reflection nebulosity that appears to be centered on, and illuminated by, the primary star. The images of Nakajima & Golimowski (1995) show that the north arm of the arc extends to the northwest to a radial distance of about 10″, which is about twice the length seen in these short *HST* exposures. Neither arm of the arc appears to coincide with the locations of high-velocity gas as traced by optical spectroscopy (Böhm & Solf 1994) or shocked molecular hydrogen emission (Herbst et al. 1997). It therefore appears to be a distinct structure that traces the boundary of dense material in the circumbinary region.

It is difficult to assess what role, if any, the companion star plays in defining the distribution of scattered light that is seen. Residual diffraction spikes pass close to the position of the companion, precluding the detection of any faint nebulosity there. The companion presumably lies behind the circumbinary material that is responsible for both its extinction and the nearby scattered visible light from T Tau N. The arc appears brighter and more truncated near the projected position of T Tau S. It is tempting to speculate that the companion might be responsible for this, perhaps because of effects of its outflow or gravity on the distribution of scattering material. Alternatively, light from T Tau S might play some role in illuminating this part of the nebula. From our data, there is no clear way to distinguish among these possibilities.

The standard paradigm for the environment around an isolated protostar is a centrifugally supported accretion disk surrounded by a more tenuous infalling envelope that extends to much higher latitudes and with bipolar cavities in the envelope cleared by the action of jets and winds from the inner disk and protostar. This paradigm must be significantly modified for the case of T Tau, because we know that two stars have formed at a separation of at least 100 AU. Presumably both stars share a common infalling envelope, the residual material of the molecular cloud core from which they formed. There is evidence to suggest that both stars drive collimated outflows that produce shocked line emission (Böhm & Solf 1994) and may carve cavities in their common envelope. Each star may have an associated accretion disk with a tidally truncated outer radius perhaps $\frac{1}{4}$ the

physical separation of the pair. They may share an outer circumbinary disk, tidally truncated at an inner radius of perhaps 4 times the binary separation. Such disk structures could survive for many dynamical timescales.

Given all of these expected features in the circumbinary environment, which is most likely to be related to the nebular arc seen about T Tau N? A natural possibility to investigate is an outflow cavity blown by winds or jets from T Tau N into the extended envelope needed to explain the *IRAS* 100 μm flux. Such a cavity would be seen via scattered light from T Tau N and could appear limb brightened. The approximate symmetry axis of the nebular arc is toward the west-northwest, requiring that the cavity and corresponding outflow be aligned near P.A. 300°. An outflow from the primary at this P.A. is consistent with the blueshifted optical emission lines and CO outflow to the west of T Tau. The southeast extension to the scattered light seen by Nakajima & Golimowski (1995) could be interpreted as part of the countercavity associated with the redshifted lobe of a bipolar outflow from T Tau N. If our scenario is correct, the circumstellar disk of T Tau N should eventually be resolved along P.A. 30°, perpendicular to the axis of the proposed outflow cavity. The separate outflow from the companion would be obscured from view in our scenario. This outflow is now known to extend north–south (Reipurth et al. 1997) and thus probably includes the bright near-infrared H_2 emission knot found by Herbst et al. (1996).

Predicted scattered light images for outflow cavities appear in the literature (Whitney & Hartmann 1993) but are presented at low spatial resolutions not well-suited for comparison with *HST* images. To test the applicability of such models to the *HST* images of T Tau, we calculated our own simple axisymmetric models for the reflected light produced when a circumstellar envelope with a cavity is illuminated by a central star. The brightness contribution of each volume element in the circumstellar density distribution is weighted according to its optical depth, extinction toward the star and toward the observer, the inverse-square law, and a Henyey-Greenstein scattering phase function. Dust properties appropriate to $\lambda = 0.5$ μm were adopted: opacity of 250 cm^2 gm^{-1}, albedo of 0.5, and asymmetry parameter $g = 0.44$. In applying such models to the T Tau images, we ignore the obvious nebular asymmetries that the axisymmetric model cannot account for. Instead we seek only to determine whether a cavity model can simultaneously reproduce the nebular arc's overall curvature, thickness, limb brightening, and location with respect to the illuminating star.

Following Whitney & Hartmann (1993), we adopt the density distribution of Ulrich (1976), which is appropriate to a collapsing envelope with rotation

$$\rho = \frac{\dot{M}}{4\pi}(GMR_c^3)^{-1/2}\left(\frac{R_c}{R}\right)^{3/2}\left(1+\frac{\sin\theta}{\sin\theta_0}\right)^{-1/2} \times \left(\frac{\sin\theta}{\sin\theta_0}+\frac{2\sin^2\theta_0 R_c}{R}\right)^{-1}, \quad (1)$$

where $\dot{M}$ is the mass infall rate, M is the mass of the central object, R_c is the centrifugal radius, R and θ are the spherical coordinate radius and latitude, and θ_0 defines the direction of the initial streamline of the infalling material. This density law is an oversimplification, since it takes no account of the binarity of the central object, but it should be an adequate description of the density near the cavity boundary. A functional form $z = ar^\beta$ was chosen for the cavity geometry in cylindrical coordinates. The bipolar cavities are considered to be completely evacuated ($\rho = 0$ for $|z| > ar^\beta$), whereas elsewhere the density is given by equation (1). We initially chose $r_c = 100$ AU, $\dot{M} = 3 \times 10^{-6}$ $M_\odot$ yr^{-1}, and $M = 2.0$ $M_\odot$ (Calvet et al. 1994). This leaves the three geometrical parameters (a, β, θ) to determine from the images.

The images should be able to constrain the range of possible parameters for the model cavity geometry. If we assume that the nebular arc corresponds to the projected cavity wall, then the small offset distance between the star and the arc of reflected light requires that we view the system nearly along the edge of the cavity wall. This can be quantified in terms of the "impact parameter" b, the observed offset between the star and the projected edge of the cavity. Geometrically, b is defined with respect to the location where the cavity's curvature brings it tangent to the observer's line of sight. The cylindrical coordinate radius at the tangent point is related to b by $r = b\beta/(\beta - 1)\sin\theta$; see Figure 3. Substituting this relation into $dz/dr = \tan\theta$, the cavity shape parameter a can be solved for in terms of θ, β, and b,

$$a = \frac{\tan\theta}{\beta}\left[\frac{(\beta-1)\sin\theta}{b\beta}\right]^{(\beta-1)}. \quad (2)$$

The value of b can be measured from the T Tau images and is about 7 pixels (45 AU). In addition to reproducing the observed impact parameter, the model cavity must reproduce the size and shape of the arc itself. This is effectively a second constraint on the three parameters, as can be seen by inspection for the case of θ near zero: the "span" of the model arc should match that of the observed nebula at a fiducial distance. By combining these two requirements, an optimized solution for the cavity geometry (a, β) can be found for any specified observer latitude θ.

Model reflection nebulae were calculated over a range of observer latitudes and their corresponding cavity shapes. Some parameter space exploration was performed manually, yielding the "optimal" result shown along with the F555W image in Figure 4. The preferred orientation of the symmetry axis is along P.A. 300°. We found that envelope

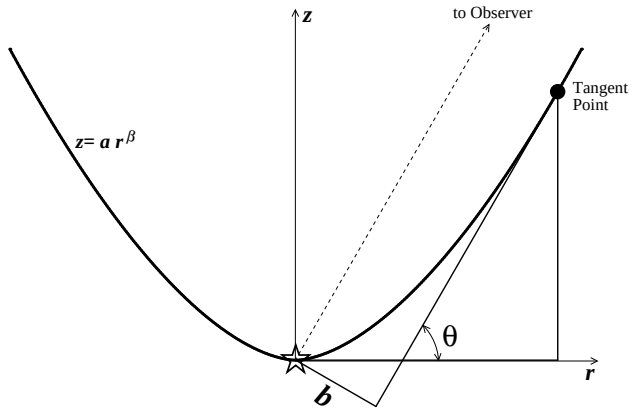

FIG. 3.—Axisymmetric cavity geometry used in the scattered light model. The observed impact parameter b between the star and the projected edge of the cavity constrains the shape parameters a, β for a specified observer latitude (see text).

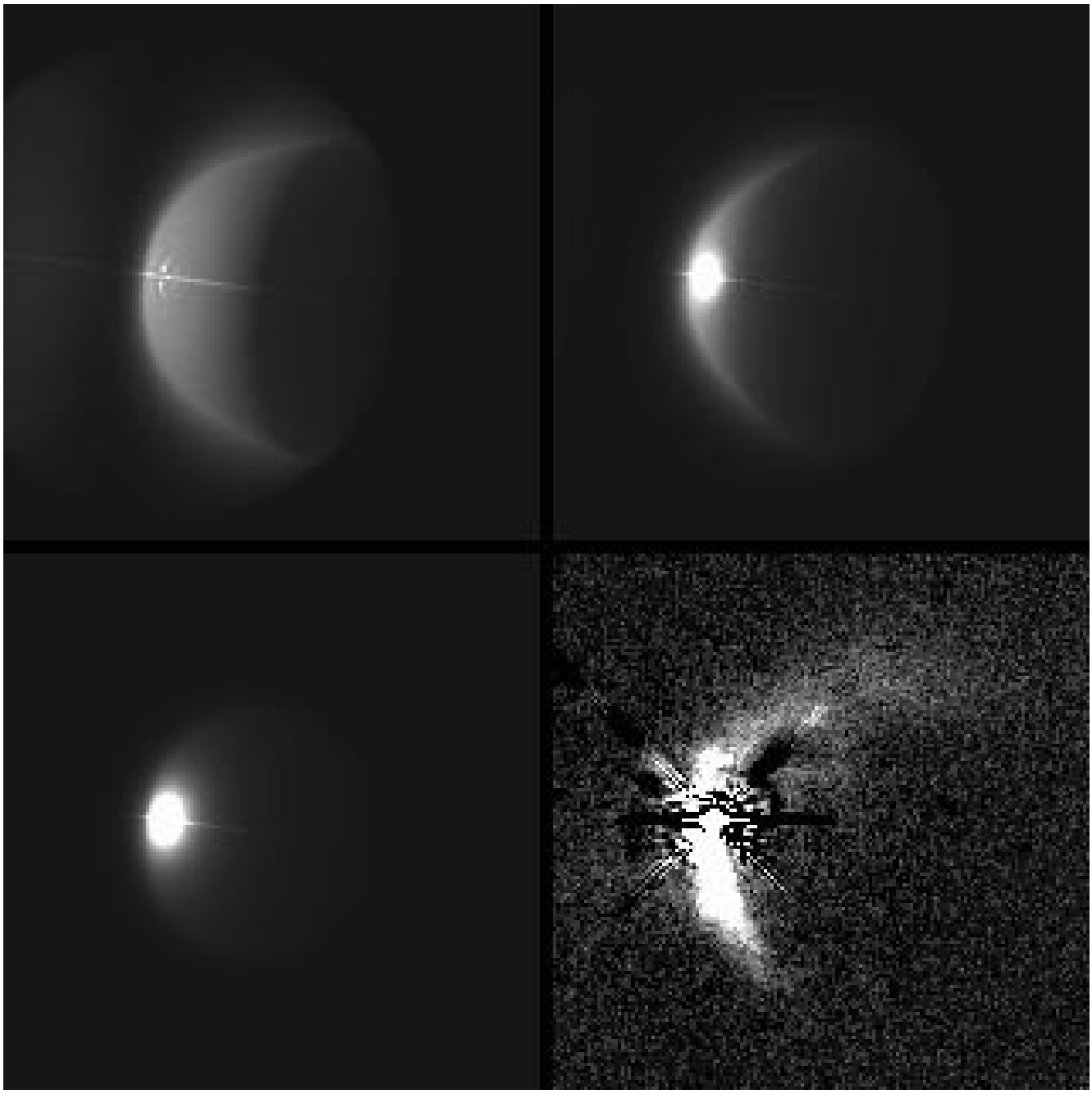

FIG. 4.—Model reflection nebulae (*top and bottom left panels*) for an axisymmetric cavity that reproduces the span, curvature, and stellar impact parameter seen in the T Tau nebular arc. The model was calculated using a 3.5 AU internal grid and resampled to the PC's resolution of 7 AU per pixel for T Tau. The *HST* F555W image is shown in the bottom right panel for comparison. Parameters of the nebula model are: *top left panel*, $\theta = 25°$, $\beta = 3.6$, $a = 3 \times 10^{-7}$; *top right panel*, $\theta = 45°$, $\beta = 1.95$, $a = 5 \times 10^{-3}$; and *bottom left panel*, $\theta = 65°$, $\beta = 1.3$, $a = 0.33$.

density normalizations less than $\dot{M} = 10^{-6}$ caused the cavity wall to become partially transparent beyond a radius of a few hundred AU. Such cases produce diffuse model nebulae that are an unsatisfactory match to the T Tau nebular arc. When viewed from low latitudes ($\theta = 25°$; Fig. 4, *upper left panel*), we found that the intrinsic curvature of the cavity must be large ($\beta > 3$) in order to reproduce the shape of the arc about T Tau N. However, this model also predicts a large envelope extinction toward the star ($A_V = 9$ mag) and a visible counternebula on the opposite side of the star from the main cavity. Since neither of these is observed, low-latitude models appear to be ruled out. From higher latitudes ($\theta = 65°$; Fig. 4, *bottom left panel*), the model images become insensitive to β because the cavity's cylindrical cross section becomes the dominant contributor to its observed curvature. At the nearly pole-on aspect suggested by the inclination of the stellar rotation axis (Herbst et al. 1986), none of our cavity models produce a nebular arc like that seen in the *HST* images. In this case ($\theta = 85°$), the models lack extended arms of reflected light, show too much circular symmetry, and formally have zero extinction toward the star. The best match to the *HST* image is obtained by our models at latitude of 45°–65°, where the nebula arms are prominent, the counternebula is not seen,

and the predicted $A_V = 3.0$ mag is close to the observed value of 2 mag.

The kinematics of the shocked optical emission lines lend support to our conclusion that the outflow cavity of T Tau N is viewed from midlatitudes. Böhm & Solf (1994) report a shocked emission knot 3″ west of T Tau N, which is within the bounds of the proposed cavity and with a radial velocity of -120 km s^{-1}. If this knot originates in a Herbig-Haro jet with typical flow speeds of 200 km s^{-1}, then its radial velocity would imply that the outflow and its aligned cavity are observed at a latitude of only 30° (the outflow is 30° from the plane of the sky). Such a jet-derived inclination seems very relevant given a jet's probable role in defining the cavity's geometry. Although our cavity models do not accommodate an inclination as low as 30°, the jet radial velocity measurements clearly favor lower latitude observing aspects than suggested by the orientation of the stellar rotation axis. Schuster et al. (1997) derive a similar inclination based on an analysis of the kinematics of the CO outflow and its relationship to NGC 1555.

Our illuminated cavity models for the T Tau nebular arc suffer from two general problems not related to any preferred orientation. First, they predict a relatively narrow limb-brightened edge for the cavity (of the order of the telescope resolution or pixel size) compared with what is actually seen. Convolution of the models with the telescope PSF falls well short of resolving this difficulty. Second, the limb-to-interior contrast of the model cavities is always less than 2. The observed contrast is greater than 4. One might think that the limb brightening could be increased by adopting a density distribution that included a swept-up shell, effectively increasing the local density of scatters at the cavity wall. However, such a model also increases the interior brightness of the cavity and leaves the limb-to-interior contrast unchanged if the cavity is axisymmetric. Before an illuminated cavity model can be declared a satisfactory match to the inner regions of Burnham's nebula, these problems need to be resolved by additional insights.

Another possibility is that the circumstellar and circumbinary disks thought to exist in the system could be related to the scattered light morphology. The circumstellar disk about T Tau N, detected but unresolved by the recent millimeter continuum observations (Akeson et al. 1998; Hogerheijde et al. 1997), is probably too small to be seen in our images. We would expect such a disk to be tidally truncated to an outer radius of order 0.″3 and thus would be completely hidden in our WFPC2 images by saturated pixels and instrumentally scattered light. A circumbinary disk would be significantly larger, perhaps comparable in scale with the nebular arc seen by *HST*. In the binary T Tauri star GG Tauri, where the binary separation is about half that of T Tau, a circumbinary disk of radius 400 AU is seen in scattered light with brightness between 10^{-3} and 10^{-4} of the stellar peak intensity (Roddier et al. 1996). A ring of this size and brightness would just be detectable in our F555W image of T Tau; however, a larger and thus fainter ring would escape detection. The arc seen in the T Tau system does not appear similar to such a ring; however, a circumbinary ring can appear as an elliptical reflection nebulosity if it is viewed from near the disk plane. Another mechanism that could produce elliptical circumbinary structures is suggested by Lubow & Artymowicz (1996): an elliptical inner hole might be carved in a circumbinary disk by dynamical effects in a highly eccentric binary system.

Although we have not calculated models for the reflected light from eccentric circumbinary disks, we briefly consider the application of such models to T Tau. Any circumbinary disk is likely to be embedded within T Tau's extended, optically thick envelope (Calvet et al. 1994). Thus the circumbinary disk in this system, if it exists at all, could be hidden from direct illumination and consequently be unobservable in reflected light. Even absent this problem, there are significant difficulties in relating the observed nebulosity to a disk model. In this system the binary components appear projected on opposite sides of the nebular arc, rather than both being enclosed by it as seen in GG Tau. This could only be reconciled to the circumbinary disk models if the disk were viewed from near its equator plane, such that the scattering layer at the disk's upper surface would happen to be projected between the two stars (one of which would be highly extincted). A face-on disk with an elliptical hole is therefore excluded. The edge-on circumbinary disk model would also require a large elliptical inner hole to match the curvature and extent of the nebular arc; and the binary would have to be near periastron, since both stars are displaced far from the center of the required arc/ellipse. This combination of special circumstances makes a disk model seem an unlikely explanation for the nebular arc, and thus some form of an illuminated outflow cavity model seems the preferable one.

5. CONCLUSIONS

1. *HST* images reveal two extensions of reflection nebulosity within 2″ of T Tau. They appear to form a single continuous nebular arc extending with some asymmetries from the north to the southwest side of the optically visible star T Tau N.

2. The nebula morphology is generally similar to models of an illuminated outflow cavity opening toward the west-northwest and viewed from intermediate latitudes. The pole-on geometry previously assumed for the system is not consistent with the observations as modeled by an illuminated outflow cavity. Although our model can reproduce the general nebula geometry, it fails to account for the large limb brightening that is observed.

3. The infrared companion T Tau S was not directly detected at visual wavelengths, suggesting an extinction of at least 7 mag. We find no evidence of an optical tertiary component in the system.

This work is supported by NASA contract NAS 7-918 to the WFPC2 Investigation Definition Team at the Jet Propulsion Laboratory, California Institute of Technology. K. R. S. also acknowledges support from the Origins of Solar Systems Research Program.

REFERENCES

Adams, F. C., Lada, C. J., & Shu, F. H. 1987, ApJ, 312, 788
Akeson, R. L., Koerner, D. W., & Jensen, E. L. N. 1998, ApJ, 505, 358
Böhm, K.-H., & Solf, J. 1994, ApJ, 430, 277
Burrows, C. J., ed. 1995, *Hubble Space Telescope* Wide Field and Planetary Camera 2 Instrument Handbook, Version 3.0 (Baltimore: STScI)
Calvet, N., Hartmann, L., Kenyon, S. J., & Whitney, B. A. 1994, ApJ, 434, 330
Dyck, H. M., Simon, T., & Zuckerman, B. 1982, ApJ, 255, L103
Ghez, A. M., Neugebauer, G., Gorham, P. W., Haniff, C. A., Kulkarni, S. R., & Matthews, K. 1991, AJ, 102, 2066
Gilliland, R. L. 1994, ApJ, 435, L63
Gorham, P. W., Ghez, A. M., Haniff, C. A., Kulkarni, S. R., Matthews, K., & Neugebauer, G. 1992, AJ, 103, 953
Herbst, T. M., Beckwith, S. V. W., Glindemann, A., Tacconi-Garman, L. E., Kroker, H., & Krabbe A. 1996, AJ, 111, 2403
Herbst, T. M., Robberto, M., & Beckwith, S. V. W. 1997, AJ, 114, 744
Herbst, W., et al. 1986, ApJ, 310, L71
Hogerheijde, M. R., van Langevelde, H. J., Mundy, L. G., Blake, G. A., & van Dishoeck, E. F. 1997, ApJ, 490, L99
Holtzman, J. A., et al. 1995, PASP, 107, 1065
Joy, A. H. 1945, ApJ, 102, 168
Kenyon, S., & Hartmann, L. 1995, ApJS, 101, 117
Krist, J. E. 1995, in Calibrating *Hubble Space Telescope*: Post Servicing Mission (Baltimore: STScI), 311
Krist, J. E., et al. 1997, ApJ, 481, 447
Levreault, R. M. 1988, ApJS, 67, 283
Lubow, S. H., & Artymowicz, P. 1996, in Evolutionary Processes in Binary Stars, ed. R. Wijers, M. Davies, & C. Taut (Cambridge: Cambridge Univ. Press), 53
Maihara, T., & Kataza, H. 1991, A&A, 249, 392
Nakajima, T., & Golimowski, D. A. 1995, AJ, 109, 1181
Nisenson, P., Stachnik, R. V., Karovska, M., & Noyes, R. 1985, ApJ, 297, L17
Reipurth, B., Bally, J., & Devine, D. 1997, AJ, 114, 2708
Robberto, M., Clampin, M., Ligori, S., Paresce, F., Sacca, V., & Staude, H. J. 1995, A&A, 296, 431
Roddier, C., Roddier, F., Northcott, M. J., Graves, J. E., & Jim, K. 1996, ApJ, 463, 326
Schuster, K.-F., Harris, A. I., & Russell, A. P. G. 1997, A&A, 321, 568
Solf, J., Böhm, K. H., & Raga, A. 1988, ApJ, 334, 229
Strom, K. M., Strom, S. E., Edwards, S., Cabrit, S., & Skrutskie, M. F. 1989, AJ, 97, 1451
Ulrich, R. K. 1976, ApJ, 210, 377
van Langevelde, H. J., van Dishoeck, E. F., van def Werf, P. P., & Blake, G. A. 1994, A&A, 287, L25
Whitney, B. A., & Hartmann, L. 1993, ApJ, 402, 605